Pergamon

Chaos, Solitons & Fractals Vol. 7, No. 2, pp. 165–175, 1996

0960-0779/96 $15.00 + 0.00

0960-0779(95)00064-X

Nonmonotonic Maps and Related Bifurcations in Laser Accelerators*

T. S. CAETANO, F. COUTO, G. CORSO, R. PAKTER, L. G. BRUNNET and F. B. RIZZATO

Instituto de Física, Universidade Federal do Rio Grande do Sul, Caixa Postal 15051, 91501-970 Porto Alegre, RS, Brazil

(Accepted 27 June 1995)

Abstract—In this paper we analyze the orbital dynamics of electrons in a laser accelerator whose high-frequency laser wave is slowly modulated both in space and time. Slow modulations are a natural result of modulational instabilities and wave–particle energy exchanges, and for typical system parameters we focus our study on stability and bifurcations of periodic orbits. It is found out that the orbital nonlinear frequencies are nonmonotonic functions of the system energy. This leads to the appearance of peculiar reconnection processes and associated inverse saddle-node bifurcations, in addition to the more usual period doubling cascades preceding chaos.

1. INTRODUCTION

There has been a growing interest in the study of stochastic relativistic interactions involving magnetized electrons and electromagnetic waves. This is so because relativistic particles are likely to absorb large quantities of electromagnetic energy when the wave–particle interaction is adequately tuned. The wave–particle energy exchange can be either chaotic or regular depending on the degree of integrability of the model one is dealing with. Fully integrable models provide regular acceleration but even small nonintegrable effects may cause the process to become chaotic. Chaotic acceleration can be even dominant in view of the ineffectiveness of regular processes occurring under a variety of conditions.

One particularly promising configuration for laser acceleration is the cyclotron-resonance laser accelerator (CRLA) [1], where a laser wave may transfer a large amount of energy to a beam of electrons gyrating in a guided magnetic field. This large amount of transferred energy takes place because of the autoresonance mechanism [2] whereby an initial wave–particle synchronism may be self-sustained to a large extent throughout the accelerating period.

If the amplitude of the laser is approximately constant during the accelerating process, one shows that the electronic dynamics is exactly integrable. However, as analyzed in a number of recent simulations [2, 3], the laser amplitude usually undergoes appreciable fluctuational levels in tuned systems. When this happens, the process can still be shown to be regular if particles are launched with such small initial energies that a strong phase-bunching mechanism reduces the effective dimensionality of the system inhibiting the development of nonintegrable features. The real transition to nonintegrability occurs when waves and particles are tuned to each other but the initial particle energy is not small enough that phase-bunching takes place—then the system may become chaotic.

*Communicated by Professor C. Grebogi.

Chaos in CRLAs is a possibility recently investigated in Pakter *et al.* [4]. In the model analyzed, the amplitude of the laser field undergoes *temporal* slow modulations, with these modulations causing the appearance of series of period doubling bifurcations leading to chaotic regimes. These time-like amplitude variations can be used to describe situations of physical interest, whenever the wave–particle interaction region is sufficiently short that spatial effects are negligible; this would be the typical case of small laboratory accelerators. On the other hand, when the interaction region becomes much longer, some mixed space-time effects should be included in order to model the relevant fluctuational and modulational processes more correctly [5].

Astrophysical accelerating systems are good examples of these long-sized systems, with the respective wave–particle configuration very similar to the one we are interested in: electrons moving along magnetic field lines and interacting with collinear high-frequency electromagnetic waves. As for the electromagnetic waves, they are generally modulationally unstable [6], undergoing mixed modulations in time and space. Even laboratory settings can cause substantial space–time modulations on the laser signal. In fact, some recently proposed schemes of adiabatic tuning make use of long accelerating lengths such that the effect of long range inhomogeneities can not be discarded [7].

The purpose of this paper is, therefore, to analyze chaos, orbital stability, and orbital bifurcations preceding chaos in a CRLA whose laser wave is modulated both in time and space. We shall see that the related nonlinear dynamics reveals some new features. It is known that the nonlinear dynamics of various Hamiltonian systems can be frequently represented by monotonic twist maps [8] where the nonlinear orbital frequency of the system is a monotonic function of energy or action. In contrast, as we shall see here, the present system manifests characteristics of nonmonotonic twist maps, where the orbital frequency does not depend monotonically on energy [9–11]. We shall see how this peculiar characteristic affects the stability and bifurcations of the various periodic orbits immersed in the phase-space. Dispersive characteristics of the laser wave are known to be of central relevance and shall, therefore, be retained in the model. If dispersion were absent full autoresonance would be attained; the presence of dispersion saturates the accelerating process providing one basic mechanism to generate nonlinear resonant islands and, subsequently, chaos.

The paper is organized as follows: in Section 2 we specify the model; in Section 3 we perform various simulations in order to determine the structure of the phase-space and the stability and bifurcations of various periodic orbits; and in Section 4 we conclude the work.

2. THE MODEL

Let us start by introducing the Hamiltonian of a test particle submitted to the combined action of a constant guiding magnetic field and an intense electromagnetic mode. Both the guided field and the wave vector of the fluctuating field are assumed aligned with the z axis of the chosen reference frame. The magnetic field is written as $\boldsymbol{B}_o = B_o\hat{z}$ and the vector potential of the wave, $\mathbf{A}_w$, as

$$\frac{e}{m_e c^2}\mathbf{A}_w \equiv -\tfrac{1}{2}\sqrt{(\rho)}[\cos(kz - \omega t)\hat{\mathbf{x}} + \sin(kz - \omega t)\hat{y}], \tag{1}$$

where $\rho = \rho(z, t) = \rho_o(1 + \varepsilon\cos(Kz - \Omega t))$ $(\varepsilon \leqslant 1)$ is slowly modulated in space and time because K and Ω appear as a small modulational wave vector and frequency, $K \ll k$ and $\Omega \ll \omega$, where k and ω are the fast wave vector and frequency of the carrier wave,

respectively. The electron charge is denoted by e, m_e is its mass, c is the velocity of light. The single particle Hamiltonian

$$\frac{H}{m_e c^2} = \left[1 + \left(\frac{P_x}{m_e c} + \sqrt{(\rho)}\cos(kz - \omega t)\right)^2 + \left(\frac{P_y}{m_e c} - \frac{eB_o x}{m_e c} + \sqrt{(\rho)}\sin(kz - \omega t)\right)^2 + \frac{P_z^2}{m_e^2 c^2}\right]^{1/2} \quad (2)$$

can be cast in the nondimensional guiding-center resonant form

$$H = -\omega J - \frac{\Omega}{K} P_z + \sqrt{[1 + 2J + (P_z + kJ)^2 + \sqrt{(\rho)} J\cos(\phi) + \rho]}, \quad (3)$$

if one observes the following steps:

(i) define $\omega_{co} \equiv eB_o/m_e c$;
(ii) normalize $\omega/\omega_{co} \to \omega$, $\omega_{co} t \to \mathrm{t}$, $(\omega_{co}/c)\mathbf{r} \to \mathbf{r}$, $\mathbf{P}/m_e c \to \mathbf{P}$, and $H/m_e c^2 \to H$;
(iii) introduce canonical guiding-center coordinates $P_x = \sqrt{(2J)}\cos\phi$ and $x - P_y = \sqrt{(2J)}\sin\phi$;
(iv) perform a canonical transformation removing explicit fast time dependence: $H \to H' = -\omega J + H$, $J \to J' = J$, $\phi \to \phi' = \phi + (kz - \omega t)$, $P_z \to P_z' = P_z - kJ$, $z \to z' = z$;
(v) perform an additional canonical transformation to remove explicit slow time dependence: $H' \to H'' = H' - (\Omega/K)P_z'$ and $z' \to z'' = z' - (\Omega/K)t$, all other variables remained unaltered.

In (3), $\rho = \rho_o[1 + \varepsilon\cos(Kz)]$ and primes have been dropped.

Hamiltonian (3) is constant for time but is 2-degrees-of-freedom, with the respective pair of conjugated variables as (J, ϕ) and (P_z, z). Following the ideas of Ref. [12], for instance, one can now reduce the dimensionality to 1.5-degrees-of-freedom such that the resulting system behaves similarly to the more tractable case of an integrable 1-degree-of-freedom plus some time dependent external perturbation, the '1/2'-degree-of-freedom. What has to be done is just to invert relation (3) in order to write $P_z = P_z(H, J, \phi, z)$. Then, as shown in the reference above, the ensuing dynamics is governed by the pair of canonical equations:

$$d_z J = -\partial_\phi(-P_z), \qquad d_z \phi = \partial_J(-P_z), \quad (4)$$

with $d_z \equiv d/dz$ and $\partial_{J,\phi} \equiv \partial/\partial J, \phi$; in other words, $-P_z(H, J, \phi, z)$ is the Hamiltonian in a representation where z plays the role of time and H is a constant momentum.

One now assumes $\omega = k(1 + f(k))$ with $f \neq 0$ therefore measuring the wave dispersion in the system. If f were set to zero, one would have vacuum propagation which is not quite as realistic, as advanced in the Introduction. The importance of considering nonvanishing values of f relies on the central role played by dispersion in determining the saturation levels of the interaction.

Then, according to vast material on astrophysics and laboratory acceleration, one takes $0 < f \ll 1$. This inequality reproduces physically relevant situations and justifies the choice to be made in this paper, $\Omega/K = 1$. In principle this last adopted relation should be written so as to yield the group velocity of radiation, $\Omega/K = \partial_k \omega = 1 + O(f)$, but as shall be shortly checked out, suppression of the $O(f)$-term from the above low-frequency relation, while reducing the complexity of calculations, does not remove any important feature from the model.

Taking into account these comments, it is an easy matter to effectively invert relation (3) and obtain

$$P_z = \frac{1 - H^2 + \rho + 2(1 - H\omega)J - (1 - (1 + f)^{-2})\omega^2 J^2 + 2\sqrt{(2\rho J)}\cos(\phi)}{2H + 2\left(\frac{f}{1 + f}\right)\omega J}. \quad (5)$$

This is the Hamiltonian to be investigated in what follows.

3. REGULAR AND CHAOTIC DYNAMICS

3.1. *Regular dynamics*

The regular dynamics of the model is obtained for $\varepsilon = 0$. In addition, expanding (5) in powers of f, one gets:

$$P_z = \frac{1}{2H}[\delta J - \beta J^2 + 2\sqrt{(2\rho_o J)}]\cos\phi + O(f^2), \quad (6)$$

with

$$\delta = 2(1 - \omega H) - (1 - H^2 + \rho_o)\frac{f\omega}{2H} \quad (7)$$

and

$$\beta = \frac{f\omega}{H^2}. \quad (8)$$

The singular autoresonant case is recovered when $f = 0$ and $1 - \omega H = 0$. In that case, (4) and (6) show that particles with $J(t = 0) \sim 0$ are continuously accelerated along the vertical line $\phi = \pi/2$. The inclusion of a small but nonvanishing value of f arrests unbounded acceleration. Under such conditions, one shows that the maximum value attained by the action variable such as [11]

$$J_{\max} \sim \left(\frac{\sqrt{(\rho_o)}}{f}\right)^{2/3}. \quad (9)$$

if the easily met condition $\rho_o f \ll 1$ is used to disregard the δ-term in (6).

A contour-plot of the integrable $\varepsilon = 0$-dynamics is displayed in Fig. 1. The orbit along which particles with negligible initial values of the action attain $J_{\max}$ is highlighted. It is to be noticed that such an orbit acts like a boundary, dividing the full phase-space into two distinct regions: the region of trapped orbits where ϕ excursions are bounded, and the regions of untrapped orbits where ϕ excursions are unbounded.

Within the trapping region, particles revolve around the central fixed point (CFP) with a gyrofrequency that depends upon the relative distance between this CFP and the orbit itself—we shall refer to this frequency as the internal frequency, ω_i. Besides, as far as the trapping region is concerned, one notices a strong similarity between the Hamiltonian governing the integrable dynamics, Hamiltonian (6), and the Hamiltonian studied in Ref. [11], which promptly leads us to import and quote some results derived there. Firstly, the nearer one is to the CFP, the larger the gyrofrequency—in particular, the gyrofrequency at the CFP, ω_{cfp}, is the largest. Besides, in contrast to the more usual case of pendulum-like resonant islands, as one arrives at the boundary orbit the gyrofrequency does not go to zero. This last feature has the important effect of inhibiting the appearance of boundary or separatrix chaos which otherwise needs zero-frequency orbits and the corresponding infinity

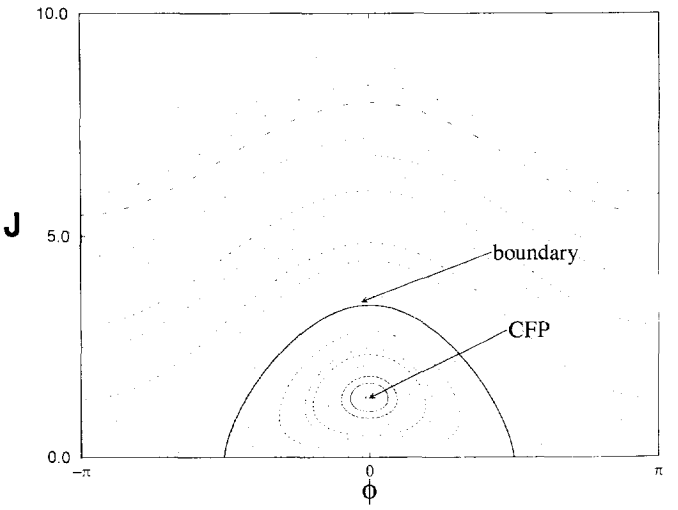

Fig. 1. Portrayal of the unperturbed phase-space; $\varepsilon = 0$, $\rho_0 = 0.002$.

of separatrix crossings and resonance overlaps to fully develop (one shows that resonance overlap generally depends on a factor $1/\omega_b$ where ω_b is the unperturbed frequency ω_i calculated at the boundary—if $\omega_b \to 0$, overlap is likely).

Now, as one abandons the trapping region, and if one is far above $J_{\max}$, from (6) one can estimate the external orbital frequency—we shall denote it by ω_e—simply as

$$|\omega_e(J)| = |\partial_J P_z| \sim |2\beta J|, \qquad \text{for } J \gg J_{\max} \tag{10}$$

a relation indicating that the orbital frequency grows in absolute value as one gradually goes into the large-J regions.

Accordingly, one concludes that the general picture goes more or less like this: the frequency is relatively high when one is very close to the CFP, and decreases as one proceeds towards the boundary. Then, as one crosses the boundary, the behavior, is reverted and the frequency starts to increase again; in other words $|\omega_{cfp}| > |\omega_b| < |\omega_e(J \gg J_{\max})|$. This amounts to saying that, as opposed to more conventional cases, one is facing a nonmonotonic dependence of frequency on, let us say, the energy of the system. As reported in recent works [9–11], and as we shall check out here, one basic implication of this nonmonotonic behavior is the appearance of direct and inverse saddle-node bifurcations of periodic orbits (or fixed points in the coming Poincaré plots) when ε is turned on, besides the conventional cascades of period doublings.

The study of the possible bifurcations is a relevant matter either from the pure theoretical point of view or, if one wishes to have an accurate idea of orbital stability in accelerating devices, from the applied point of view. We shall now turn to the pertinent analysis.

3.2. *Chaotic dynamics*

For $\varepsilon \neq 0$ the basic interest is the study of existence and stability of periodic orbits whose periods are a multiple of the basic period τ determined by the wave modulation in the form $\tau = 2\pi/K = 2\pi/\Omega$; all the forthcoming numerical investigations, like Poincaré plots and stability calculation, ought to be understood as based upon this definition for τ.

When $\varepsilon \neq 0$, two types of chains of resonant island may appear in the system: resonant

chains within the trapping region and resonant chains without the trapping region—following the nomenclature adopted for the orbital frequencies, the former kind of chain shall be referred to as internal and the latter as external.

As far as external chains are concerned, and if they are far enough from $J_{\max}$, their positioning along the J axis can be estimated from the resonance condition

$$n\omega_e(J) = mK = m\Omega, \tag{11}$$

where n, m are integers.

As for internal chains the important point to realize is that whenever

$$p\omega_{cfp} = qK, \tag{12}$$

with p, q integers, a period-p chain with p-islands bifurcates out of the CFP in the Poincaré plots. If the trapping region were a regular Chirikov-like one with zero-frequency orbits along its boundary, the behavior of internal chains would be as follows. Increase in ρ_0 would firstly push the internal chain towards the boundary. Once there, the internal chain would undergo resonance overlap with several other chains, with a subsequent full period double cascade driving a final transition to chaos [13].

The kind of trapping region we are dealing with in the present paper differs from the usual, however, in that the boundary frequency does not vanish [11], a feature inhibiting transition to chaos. As mentioned, the absence of zero-frequency orbits diminishes the possibility of island overlap and the subsequent period doubling cascades.

What has to be investigated, then, concerns the fate of resonant chains arriving at the boundary; if those chains do not undergo period doubling cascades, what kind of bifurcations, if any, do they undergo? A similar question has been analyzed, to our knowledge, in three recent papers, Refs [9–11]. What has been found in those works, particularly in the latter, can be put as follows. Some of the chains bifurcated from the CFP still undergo the usual period doublings as they approach the boundary. Others, in view of the nonmonotonic character of the system, undergo inverse saddle-node bifurcations where stable (unstable) fixed points collapse against unstable (stable) fixed points of external chains which touch the boundary simultaneously.

It is hard to predict which kind of bifurcation dominates the dynamics, although some estimates can be made for some special situations. In the present paper we shall mostly perform a numerical analysis of the relevant cases in order to see if the unusual bifurcational behavior is present.

We start by analyzing the stability properties of the CFP. The technique to be employed here and in the following, is based on a Newton-Raphson root-finder algorithm which produces the so-called stability diagrams [14]. In the stability diagrams one plots the stability index α of a particular periodic orbit as a function of any varying control parameter of the system. If $|\alpha| < 1$ the corresponding orbit is stable (elliptic fixed points) and if $|\alpha| > 1$ the orbit is unstable (hyperbolic fixed points). As mentioned earlier, two kinds of orbital bifurcations are expected to occur. In the direct or inverse period doubling bifurcations, periodic orbits undergo direct or inverse period doublings as the control parameter grows, with $\alpha = -1$ at the bifurcation point. In the inverse saddle-node bifurcation, elliptic points of a periodic orbit collapse against hyperbolic points of neighboring orbits with the same periodicity [4, 11]; in this case both orbits simply cease to exist with $\alpha = +1$ at the end point.

These are the basic characteristics we shall need to clarify the stability properties of our orbits.

Let us turn to Fig. 2. In this figure we plot $\alpha = \alpha(\rho_o)$ for various values of ε. It is seen that the CFP presents an instability window, $\alpha < -1$, as a function of ρ_o, and that the

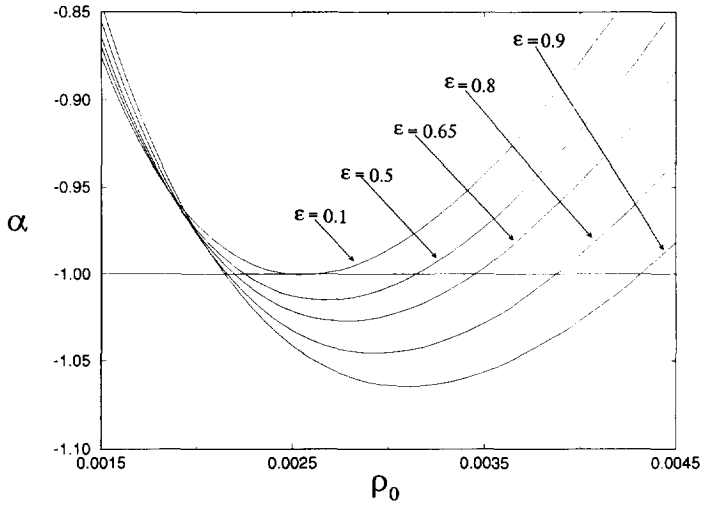

Fig. 2. Stability diagram for the Central Fixed Point, for various values of ε.

window becomes wider as the value of ε grows. One can see the window as some sort of optimal resonance region, outside which the system, or more precisely the CFP, is more or less insensitive to the effects of nonintegrable modulations. For values of ρ_o much larger than the ones presented in the figure further bifurcations may occur. However, since the phase-space is robust and essentially integrable for these larger ρ_o's, we shall focus preferential attention on the range depicted.

The instability region of the CFP is the region where it has been rendered unstable as a result of a period doubling bifurcation. Let us then proceed to investigate the behavior of the corresponding bifurcated period-2 island. To do this, we first produce a set of Poincaré plots for various values of ρ_o in order to have an overall idea of the nonintegrable phase-space along with approximated initial values for the coordinates of the various fixed points to be later used in the root-finder algorithm. The chosen value of ε is $\varepsilon = 0.9$ in what follows; this value well represents the high modulational level found, for instance, in astrophysical systems where particle acceleration is usually intense [6]. In Fig. 3 we display the sequence of plots. Figure 3(a) represents the situation before the period doubling bifurcation of the CFP. There, besides the CFP, one can also note the presence of an external period-2 chain whose existence is a relevant matter as we shall see (in the figures we make use of the compact notation $I_{e,h}$ and $E_{e,h}$ for the elliptic and hyperbolic points of the internal and external period-2 chains, respectively). In Fig. 3(b) the CFP has undergone one period doubling bifurcation originating an internal period-2 chain; it is to be noticed that the elliptic points of the external period-2 chain as well as the hyperbolic points of the internal chain are absent. Finally, in Fig. 3(c) the CFP and the external period-2 points are back to stability—besides, the internal hyperbolic points have been created. A common feature for all the situations depicted in the figures, is the relative stability of the large-J regions. In fact, the big period-1 island present in the figures can be seen as marking the transition from the chaotic region where the trapping region is immersed, to this large-J stability region. Expansion of (5) in powers of ε shows that the magnitude of the main resonances for large J's as $\varepsilon^{|m|}$ and that the distance between adjacent resonances, ΔJ, is approximately constant; $\Delta J \sim K$. As it appears these two factors combined annihilate the overlap for large J.

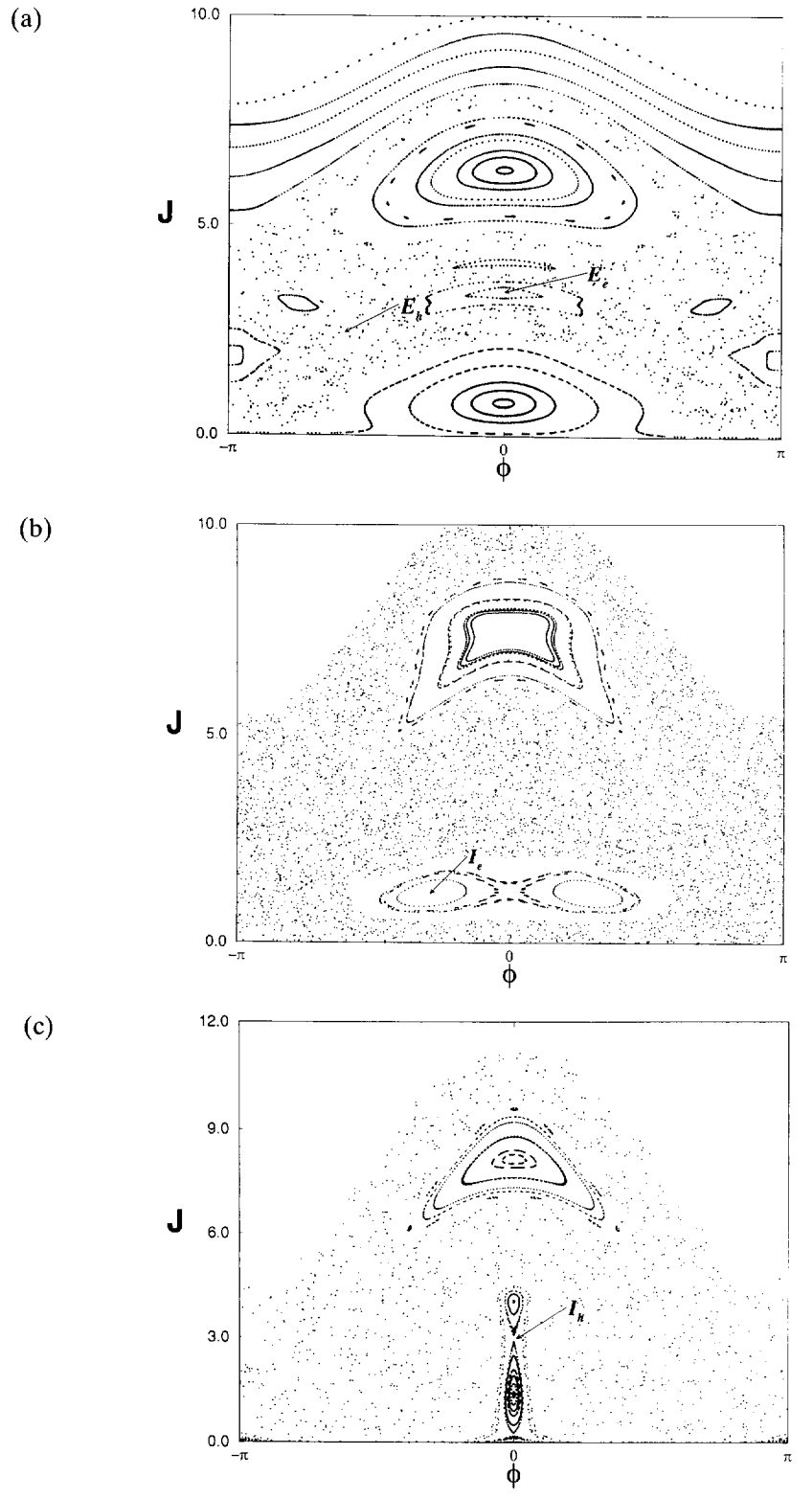

Fig. 3. A sequence of Poincaré plots for $\varepsilon = 0.9$; $\rho_o = 0.0005$ in (a), $\rho_o = 0.003$ in (b), and $\rho_o = 0.0055$ in (c).

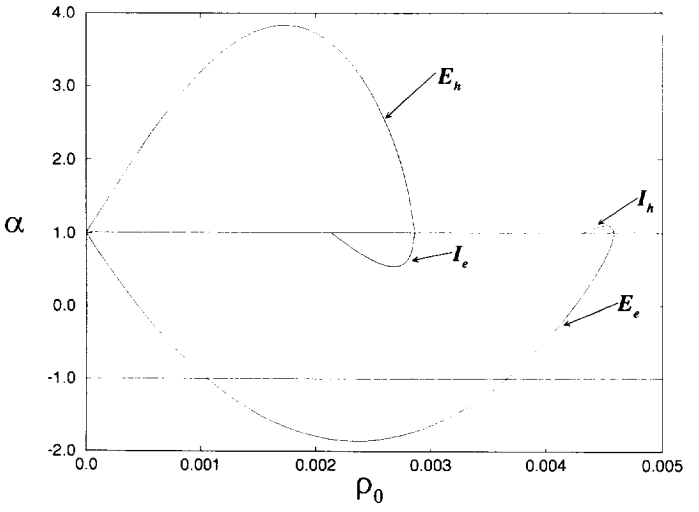

Fig. 4. The stability diagram for the stable and unstable periodic orbits of external and internal period-2 chains; $\varepsilon = 0.9$.

We now make use of all the previous information in order to follow the life-history of each fixed point of the period-2 chains. We focus on period-2 islands in view of their relevance for the overall dynamics.

Let us start with the elliptic fixed point of the internal period-2 island, I_e. As ρ_o grows for a fixed value of ε, the stability index behaves as shown in Fig. 4. It is seen that such a fixed point undergoes an inverse saddle-node bifurcation as its stability index reaches the value $\alpha = +1$. What happens at this moment is that the elliptic point collapses against the hyperbolic fixed point of the external period-2 island, E_h, as both simultaneously touch the boundary of the trapping region. We have performed simulations for various values of ε and the behavior appears to be quite insensitive on the perturbing parameter. One could see the inverse saddle-node bifurcation as interrupting the usual period doubling cascade for the CFP.

We then turn to the unstable point of the internal period-2 island, I_h. The first feature noticed from Fig. 4 is that collapse is again present, and that it occurs as the hyperbolic point hits the elliptic point of the external period-2 island, E_e. However, the collapsing value for ρ_o is not the same as previously; in fact, and as already suggested in Fig. 3, the existence region for the hyperbolic points does not coincide at all with that for the elliptic ones. In addition, the behavior of α for the external stable period-2 point as a function of ρ_o appears to be more complex. Indeed, it is seen from the figure that for such a large ε, the elliptic point undergoes a direct and inverse sequence of period doubling bifurcations before collapse. We have even kept track of some initial sequences of these bifurcations, concluding that full direct and inverse cascades appear to be present in this case. Moreover, as one increases ε for a fixed value of ρ_o, simulations not shown here indicate that full direct period doubling cascades for E_e do take place.

In general, it is thus seen that while ρ_o is a stabilizing influence on the overall dynamics, ε is a destabilizing one.

Relatively strong chaotic states can be expected when the following conditions are simultaneously fulfilled: the CFP and the elliptic points of the external period-2 chain are period doubled, and the elliptic points of the internal period-2 chain has collapsed against

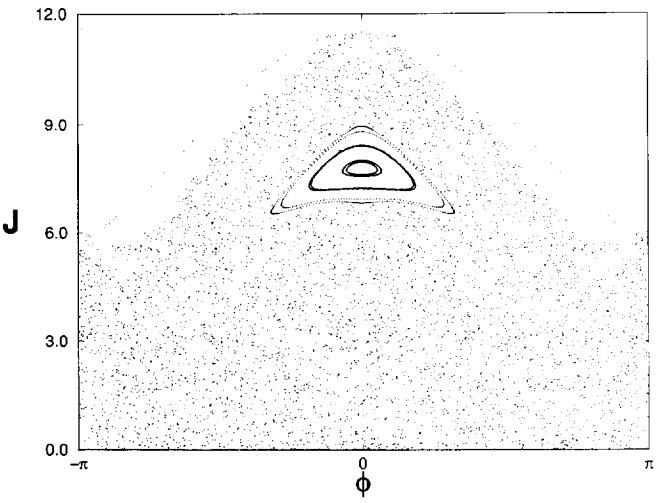

Fig. 5. Poincaré plot for $\rho_0 = 0.005$ indicating the existence of a strongly chaotic regime.

the hyperbolic points of the external period-2 chain; in that case no stable point would be present within the trapping region. Figure 5, constructed for a value of ρ_o satisfying these requirements, $\rho_o = 0.0055$, suggests this to be the case. For values of ρ_o outside the region where the conditions above are met, the phase-space tends to be more stable.

4. FINAL REMARKS

To summarize, we have performed an investigation on the nonlinear dynamics of slowly space–time modulated laser accelerators. For typical system parameters, we have observed that the unperturbed orbital frequency is a nonmonotonic function of orbital energy. This was shown to introduce some peculiar bifurcations into the general scenario of transition to chaos. Indeed, besides the more or less usual period doubling cascades, the nonmonotonic character of the system has been shown to cause periodic orbits to also undergo saddle-node bifurcations where pairs of resonant chains with the same periodicity do vanish as they collide with each other. Besides the curious aspects of the problem from the purely theoretical point of view, it is expected that the results be of relevance in the description of actual physical settings whenever the laser beams are likely to be slowly modulated. This could be the case of laboratory systems where beams are externally modulated by varying control parameters (like the waveguide radius, for instance) [7] or the case of astrophysical particle jets where the radiation beam is both self-modulated [6, 15] or modulated by wave–particle effects [3].

Acknowledgements—This work was partially supported by CNPq (Coordenadoria de Desenvolvimento Científico e Technológico), FINEP (Financiadora de Estudos e Projetos), and PROPESPUFRGS (Pró-reitoria de Pesquisa—Universidade Federal do Rio Grande do Sul), Brazil. Numerical computing was performed on the CRAY YMP-2E at the Universidade Federal do Rio Grande do Sul Supercomputing Center.

REFERENCES

1. P. Sprangle, L. Vlahos and C. M. Tang, A cyclotron resonance laser accelerator, *IEEE Trans. Nucl. Sci.* **NS-30**, 3177 (1983).
2. C. Chen, Theory of electron-cyclotron-resonance laser accelerators, *Phys. Rev. A* **46**, 6654 (1992).

3. R. Pakter, R. S. Schneider and F. B. Rizzato, Influence of wave dispersion on the self-consistent dynamics of cyclotron-laser systems, *Phys. Rev. E* **47**, 3787 (1993); *ibid*, Effects of frequency mismatch and wave dispersion on a self-consistent Hamiltonian model for an arbitrary amplitude cyclotron resonance laser accelerator, *Phys. Rev. E* **49**, 1594 (1994); and R. Pakter and F. B. Rizzato, Numerical simulations of mismatch and dispersive effects on cyclotron resonance lasers accelerators with arbitrary amplitudes, *Phys. Scripta* **48**, 598 (1993).
4. R. Pakter, G. Corso, T. S. Caetano, D. Dillenburg and F. B. Rizzato, Bifurcations leading to stochasticity in a cyclotron-master system, *Phys. of Plasmas* **1**, 4099 (1994).
5. L. G. Brunnet, H. Chaté and P. Manneville, Long-range order with local chaos in lattices of diffusively coupled ODEs, *Physica D* **78**, 141 (1994).
6. A. C.-L. Chain and C. F. Kennel, Self-modulational formation of pulsar microstructures, *Astrophys. Space Sci.* **97**, 9 (1983).
7. L. Friedland, Spatial autoresonance cyclotron accelerator, *Phys. of Plasmas* **1**, 421 (1994).
8. A. J. Lichtenburg and M. A. Lieberman, *Regular and Stochastic Motion*. Springer, Berlin (1983).
9. J. E. Howard and J. Humphreys, Nonmonotonic twist maps, *Physica D* **80**, 265 (1995).
10. G. Oda and I. Caldas, Reconnection in magnetic field lines, accepted for publication in *Chaos, Solitons and Fractals*.
11. G. Corso and F. B. Rizzato, Hamiltonian bifurcations leading to chaos in a low-energy relativistic wave-particle system, *Physica D* **80**, 296 (1995).
12. N. M. Kroll, P. L. Morton and M. N. Rosenbluth, Free-electron laser with variable parameter wigglers, *IEEE Journal of Quantum Electronics* **QE-17**, 1436 (1981).
13. E. Ott, *Chaos in Dynamical Systems*. Cambridge (1993).
14. G. Polymilis and K. Hyzanidis, Transition to stochasticity in the relativistic and the nonrelativistic versions of a dynamical system, *Phys. Rev. E* **47**, 4381 (1993).
15. G. I. de Oliveira, F. B. Rizzato and A. C.-L. Chian, Length scale, quasiperiodicity, resonances, and separatrix crossings in the weakly relativistic Zakharov equations, accepted for publication in *Phys. Rev. E*.